Demonstration of Electron-Bernstein-Wave Heating in a Tokamak via *O-X-B* Double-Mode Conversion

A. Mueck,[1] L. Curchod,[1] Y. Camenen,[1] S. Coda,[1] T. P. Goodman,[1] H. P. Laqua,[2] A. Pochelon,[1] L. Porte,[1] and F. Volpe[2]
[1]*Ecole Polytechnique Fédérale de Lausanne (EPFL), Centre de Recherches en Physique des Plasmas, Association EURATOM, CH-1015 Lausanne*
[2]*Max-Planck-Institut für Plasmaphysik, EURATOM Assoziation, D-17491 Greifswald*
(Received 7 August 2006; published 27 April 2007)

The first demonstration of electron-Bernstein-wave heating by double-mode conversion from the *O* to the *X* mode in an overdense *H*-mode tokamak plasma has been achieved in the Tokamak à Configuration Variable device. This technique overcomes the upper density limit experienced by conventional microwave heating. The sensitive dependence of the *O-X* mode conversion on the microwave launching direction has been verified experimentally, and localized power deposition consistent with theoretical predictions has been observed at densities well above the conventional cutoff.

DOI: 10.1103/PhysRevLett.98.175004 PACS numbers: 52.35.Hr, 52.35.Mw, 52.50.Sw, 52.55.Fa

A high plasma density will be beneficial to the fusion power yield in a thermonuclear reactor both directly, by increasing the reaction rate, and indirectly, by increasing the plasma confinement, according to well-established experimental observations. High plasma densities, however, hamper one of the main plasma heating techniques, electron cyclotron resonance heating (ECRH), which employs externally launched electromagnetic waves in the microwave range. This technique is particularly valuable when very localized power deposition is required, such as for local instability suppression, but becomes generally impossible above a density threshold [1], corresponding to the appearance of a cutoff layer that reflects the wave before it can reach the resonance where it can transfer its energy to the plasma. The only exception to this limitation is provided by the electron-Bernstein-wave (EBW) [2], an electrostatic mode that has no density cutoff but cannot exist in vacuum, and can therefore only be excited by mode conversion from an electromagnetic mode. A double-mode-conversion process [3] offers the best practical possibility for electron-Bernstein-wave heating (EBWH), launched from the low field side (LFS) of a toroidal magnetic confinement device. At a particular launching angle, a quasicircularly polarized ordinary-mode (*O*-mode) wave at angular frequency ω converts to extraordinary (*X*) mode at the plasma cutoff. The mode-conversion power transmission function T [4] is given by

$$T(N_\perp, N_\parallel) = \exp\left\{-\pi k_0 L_n \sqrt{\frac{Y}{2}}[2(1+Y)(N_{\parallel,\mathrm{opt}} - N_\parallel)^2 + N_\perp^2]\right\}, \quad (1)$$

where $L_n = n_e/(\partial n_e/\partial x)$ is the density-gradient scale length, $N_\perp$ and $N_\parallel$ are the refraction indices perpendicular and parallel to the magnetic field, $Y = \omega_{ce}/\omega$, and ω_{ce} is the electron cyclotron (EC) angular frequency. Only for the optimum $N^2_{\parallel,\mathrm{opt}} = Y/(Y+1)$, equivalent to a specific injection angle, and $N_\perp^2 = 0$ can the *O*-mode wave be completely converted to *X* mode. The fraction of the radiation that is not mode converted is reflected back toward the plasma edge and escapes the plasma. The width of the transmission function also translates into an angular tolerance for the wave injection, which decreases with L_n; that is, a steep density gradient facilitates the *O-X* conversion. After this first mode conversion, the wave propagates back toward the plasma edge until it encounters the upper hybrid layer, where a second mode conversion from *X* wave into the Bernstein (*B*) wave occurs. This conversion occurs with near 100% efficiency in a hot plasma [3]. The *B* mode then propagates to the plasma center and is absorbed at harmonics of the electron cyclotron resonance. The *O-X-B* heating scheme was successfully demonstrated for the first time in the stellarator W7-AS [5], in the high-density high-confinement mode. In spherical tokamaks with low aspect ratios and in reversed field pinches, electron Bernstein emission measurements are reported [6–8]. Bernstein wave heating was demonstrated in a tokamak below the *O*-mode density cutoff using the *X-B* scheme, using high field side (HFS) launch [9]. Overdense plasma heating was demonstrated in a spherical tokamak using the *X-B* scheme from the LFS with the *X* mode tunneling through the evanescent layer with highly reduced L_n due to a local limiter [10]. In this Letter, the first demonstration of EBWH in a conventional-aspect-ratio tokamak, via *O-X-B* double-mode conversion, is presented. The high-density gradient required for this scheme is obtained by operating in the high-confinement mode (*H* mode) [11].

The experiments are performed in the Tokamak à Configuration Variable (TCV) (aspect ratio $R/a = 0.88\ \mathrm{m}/0.25\ \mathrm{m} = 3.5$, magnetic field $B_T \leq 1.54$ T). The TCV second-harmonic electron cyclotron heating system is equipped with six gyrotrons each producing microwaves with a power of 500 kW at the frequency $f = 82.7$ GHz in *X* or *O* mode. The microwaves are injected through launchers, equipped with focusing mirrors, that can be rotated in two dimensions: the beam direction is then parametrized by two injection rotation angles, which will henceforth be

termed the poloidal and toroidal angles. The six launchers are distributed between two different locations in the poloidal plane. A discharge with a central density $n_{e0} \geq 1 \times 10^{20}$ m^{-3} was developed in the H-mode regime, characterized by a steep density gradient at the plasma edge. Since the efficiency of the O-X conversion decreases with increasing density scale length [see Eq. (1)], the plasma cutoff, where the O-X conversion occurs, has to be located in this high-density-gradient region. Such a scenario was achieved in TCV in nonstationary discharges with constantly rising density.

The fraction of the power converted from O to X mode for such an H-mode discharge is calculated with the nonrelativistic ART ray-tracing code which includes mode conversion and electron-Bernstein-wave propagation and absorption [12,13]. The calculation is performed using single-ray propagation and therefore does not take into account the finite width (both spatial and spectral) of the beam. The density profiles are taken from experimental Thomson scattering data. The calculation yields an angular window in poloidal and toroidal angles for the optimum O-X conversion. To verify this angular window experimentally, the launcher angles were scanned around the calculated optimum angles in steps of three degrees on a shot-to-shot basis. Modulated O-mode EC waves were injected with $P \sim 500$ kW, a modulation frequency of $f_{\mathrm{mod}} = 143$ Hz, and a 6% duty cycle. The low duty cycle was chosen to protect equipment from excessive microwave power impact when the power reflection is high. Because of the resulting low average injected power, a quantitative measurement of the variation in the plasma stored energy proved impossible, as the temperature variation is smaller than the error bars in the Thomson scattering measurement. The power absorption was evaluated therefore by measuring the EC radiation escaping the plasma ("stray" radiation), which constitutes the non-absorbed-power fraction and is therefore a very sensitive diagnostic to measure the O-X conversion efficiency. Stray measurements are performed with semiconductor diodes, distributed at different locations around the torus to ensure that the observed behavior is not a local phenomenon and is a reliable measurement of the total reflected EC power.

Semiperiodic instabilities, edge localized modes (ELMs), occur in the H-mode regime and transiently reduce the density gradient, modifying the conversion efficiency and the optimal injection angle. This effect must therefore be taken into account in the experiment. ELMs are most easily visualized as spikes on a trace of D_α light emission, generated by the recombination of deuterium particles at the plasma edge. In Fig. 1, the stray radiation is shown, normalized to its maximum level during the discharge. The periodic spikes in this trace correspond to the short EC pulses. The measurement was taken by a diode nearly diametrically opposed to the launching location. A D_α emission trace is superimposed on the stray signal to show the strong influence of ELMs on the wave absorption. The stray power level, as measured during the short EC pulses, is lower during the initial ELM-free phase than after ELMs start occurring, consistent with power reflection being increased by the higher density scale length (increased by a factor of 6 in 34 ms) as well as the lower central density induced by ELMs. This results in a smaller angular window for the O-X conversion, shown by ART calculations. When the ELMs stop, the plasma reverts to an ELM-free phase. The stray radiation returned to the initial low level ~100 ms after the last ELM, as the density scale length L_n increased gradually, resulting again in good absorption conditions. The dependence of the stray signal on ELMs and density is a first qualitative indication of successful O-X conversion. In order to determine the dependence of the stray power on the launcher angles, similar conditions had to be reproduced from shot to shot. The time windows for identification of the stray level are chosen in ELM-free periods, with the central density $n_{e0} \sim 1.4 \times 10^{20}$ m^{-3}. In Fig. 2(a), the average stray power value, normalized to the highest signal during the discharge, is plotted against the poloidal launcher angle. A clear minimum in the stray level is observed, correspond-

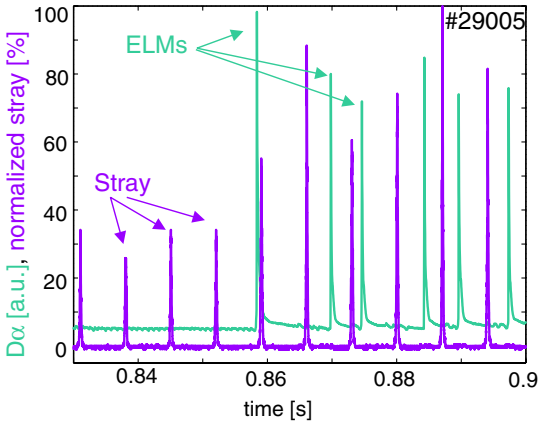

FIG. 1 (color online). Normalized stray radiation power and D_α light emission. Edge localized modes can strongly influence the stray radiation. The stray power, measured during the short EC pulses, rises from 30% to 80%.

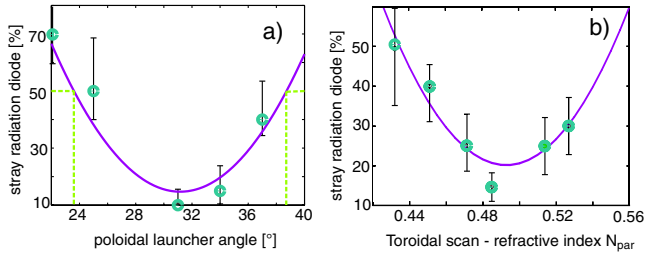

FIG. 2 (color online). Normalized stray radiation power versus (a) poloidal launcher angle (with constant toroidal launcher angle) and (b) parallel refractive index of the injected microwave beam for a toroidal scan with constant poloidal angle; the solid curves represent polynomial regression fits to the data. A clear minimum in the stray radiation is found in both scans, which is equivalent with the optimum launcher angle and parallel refractive index.

ing to a maximum in the EC power absorption. In Fig. 2(b), the stray level in a toroidal scan is shown versus the parallel refractive index of the injected microwave beam. A minimum in the stray level is found as a function of the poloidal and toroidal launcher angle as well as in function of the parallel refractive index for both poloidal and toroidal angle scans. A similar result is obtained by injecting the EC waves through a launcher located at different poloidal and toroidal locations. In Fig. 3, both the poloidal and toroidal angle scans are superimposed as violet dots to the angular window of an ART simulation, represented by contours of constant *O*-*X* conversion efficiency. The interpolated minimum in the stray radiation intensity, equivalent to the maximum ECRH power absorption, is marked by a green dot. Its position differs only by about 3° from the predicted one. This small deviation can originate from the resolution of the scan in Fig. 2 and the uncertainty in the reconstruction of the magnetic equilibrium, used by ART. The equilibrium can have errors of ±1 cm in the vertical position of the plasma axis. When such a variation is applied to the ART simulation, the optimum angle varies by ∼ ± 1°. A more significant difference exists between the angular widths of the experimental and theoretical conversion-efficiency functions. The experimental full width at 50% absorption, as indicated by the dashed (green) lines in Fig. 2(a), is approximately 15° for the poloidal launcher angle and 21° for the toroidal launcher angle, whereas their theoretical counterparts, determined from Fig. 3, are approximately 6° and 11°, respectively. This discrepancy is not surprising in view of the finite width of the EC beam and the spread in its wave-number spectrum, which can be expected to broaden the width of the conversion-efficiency function, as well as to reduce its absolute value. This is also consistent with the finite value of the experimental minimum stray power, i.e., with the peak absorbed-power fraction being less than 100%. A more realistic modeling of the experiment will require a ray bundle simulating a finite microwave beam.

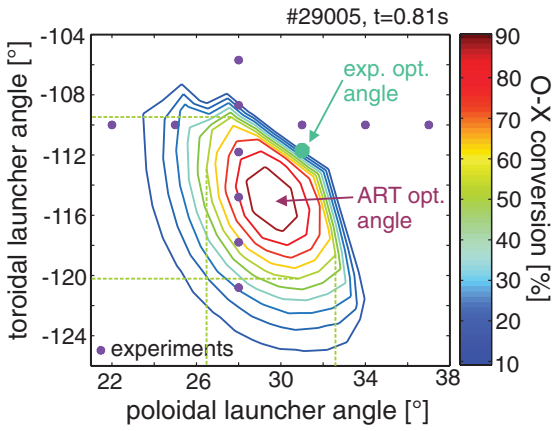

FIG. 3 (color). Contour plot of calculated *O*-*X* conversion efficiency versus poloidal and toroidal launcher angles. The innermost contour indicates 90% *O*-*X* conversion, the outermost contour 10%. The superimposed points give the launcher angles of the experimental scans (see Fig. 2); the green point corresponds to the extrapolated optimum experimental angles and is within 3° of the calculated angles.

Having determined the optimum angle experimentally, the duty cycle was then increased to 46% to achieve bulk heating and investigate global and local power deposition. The EC waves were modulated at 182 Hz, to minimize spectral overlap with the so-called sawtooth instability at $f_{ST} \sim 110$ Hz and with its harmonics. A basic cross-check of the conversion scheme can be performed by simply comparing the stray radiation level when power is injected in *O* mode (in the vicinity of the optimum launcher angles) and in *X* mode: *X*-mode injection is expected to result in total reflection from the *X*-mode cutoff layer. With alternative injection of *O* and *X* mode during ELM-free periods in similar operating conditions, the stray level with *O*-mode injection is indeed only 40% of the *X* mode stray level. The average overall absorbed power can be assessed quantitatively by means of a diamagnetic flux loop, measuring the toroidal magnetic-flux variation, which is related to the plasma stored energy [14]. Since the modulation period is shorter than the characteristic transport loss time scale (energy confinement time $\tau_e \sim 50$ ms), the modulated stored-energy signal can then be used to derive the absorbed power. An average EC power absorption of about 60% of the total injected power is measured. A total power-absorption measurement naturally cannot conclusively prove the nature of the absorption mechanism, which could involve edge absorption of waves generated by nonlinear wave-wave coupling as well as absorption of waves multiply reflected from the vacuum vessel. A determination of the power deposition location is therefore essential.

In Fig. 4, the ART calculation of the wave path in the poloidal and the toroidal projections is shown for a case with power deposition close to the plasma edge. The wave propagates to the plasma cutoff at $\rho_\psi \sim 0.9$, is mode converted into *X* mode, continues its path to the upper-hybrid resonance, where it is converted into the Bernstein mode. As shown in Fig. 5(b), the beam power is deposited at $\rho_\psi \sim 0.78$, i.e., well inside the plasma cutoff layer located at $\rho_\psi \sim 0.9$. The deposition location is determined experimentally by inspecting the spatial distribution of the modulated component of a line-integrated soft-x-ray emission

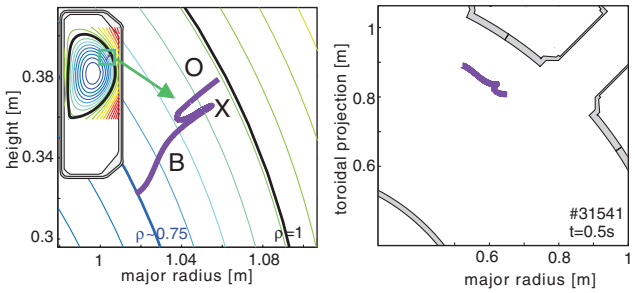

FIG. 4 (color). ART calculation of the wave path in the (a) poloidal and (b) toroidal projections, including the *O*-*X*-*B* double-mode conversion.

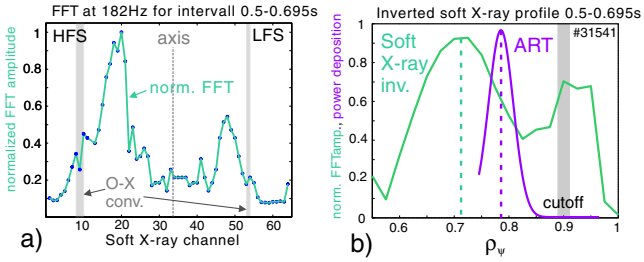

FIG. 5 (color online). (a) Normalized FFT amplitude of the line-integrated soft-x-ray time trace at the modulation frequency of $f = 182$ Hz versus the chord number. (b) Local soft-x-ray emissivity derived by integral inversion from the line-integrated soft-x-ray signals, and normalized density of deposited beam power, calculated by ART: the power is absorbed at $\rho_\psi \sim 0.78$, well inside the plasma cutoff at $\rho_\psi \sim 0.9$.

signal, detected by a multiwire chamber proportional detector with multiple lines of sight viewing in the vertical direction and covering the entire plasma cross section. Soft-x-ray emissivity has a monotonically increasing dependence on electron temperature, and again because of the short modulation period the spatial location of the modulated emissivity can be taken as a reliable measure of the power deposition location. In the soft-x-ray signals, the EC modulation is seen on several channels on both the HFS and the LFS of the magnetic axis. In a fast Fourier transform (FFT) of the time traces of the 64 channels, a clear peak at the EC modulation frequency is visible. To find the deposition location of the EBW, the FFT amplitude of the peak at the modulation frequency is plotted against the soft-x-ray channel number in Fig. 5(a). Two clear maxima in the amplitude are visible. These broad spatial peaks correspond to chords whose minimum radial coordinate (at the point at which they are tangent to the flux surface) is $\rho_\psi \sim 0.65$, on both the HFS and the LFS. The maximum on the HFS is more pronounced owing to the combined effects of line integration and plasma triangularity, which causes an in-out asymmetry, as shown in Fig. 4(a). The final step in determining the deposition location is an integral inversion of the line-integrated soft-x-ray signals to derive the local emissivity distribution. This is accomplished under the assumption of poloidal isotropic emissivity by employing the Fisher regularization algorithm. In Fig. 5(b), the FFT amplitude of the inverted signal at the EC modulation frequency is shown. Two peaks are visible. The more pronounced peak of the FFT amplitude after the inversion is located at $\rho_\psi \sim 0.7$. This experimental peak deposition location is close to the calculated one at $\rho_\psi \sim 0.78$. The slight difference may be attributed again to uncertainties in the equilibrium reconstruction and in the density-gradient measurement. The smaller peak is situated outside the plasma cutoff. Some power can be absorbed by multipass absorption after incomplete *O-X* conversion. The closeness of the theoretical and experimental deposition locations constitutes strong proof that the *O-X-B* mechanism is at play and that the plasma is being heated by EBWH inside the plasma cutoff.

In conclusion, the first demonstration of EBW heating by *O-X-B* double-mode conversion in an overdense conventional-aspect-ratio tokamak has been obtained in the TCV device. Microwave stray radiation measurements were used to assess the reflected, non-mode-converted power fraction, in discharges with modulated EC wave injection with a low duty cycle. The theoretically predicted dependence of the *O-X* conversion on the initial beam direction was verified experimentally in 2D launcher angle scans by comparison with numerical single-ray tracing calculations. The values of the optimum angles are correctly reproduced within the experimental uncertainties, whereas the angular width of the mode-conversion efficiency is underestimated by the calculation. This discrepancy is attributed to the finite beam width, which can be simulated realistically only with a multiple-ray calculation. Higher-duty-cycle modulated EC waves, injected in the optimum direction, were used to perform bulk electron-Bernstein-wave heating experiments. An average absorbed-power fraction of about 60% was measured at densities located well above the cutoff value for conventional microwave heating. The spatial distribution of the power absorption was determined experimentally by FFT analysis of soft-x-ray emissivity, and the location of the peak in the absorption profile was also found to match the value predicted by ray tracing within the experimental uncertainties.

The ART software has been acquired and used with the permission of IPP-Garching. This work was partly funded by the ''Fonds National Suisse de la Recherche Scientifique'' and supported by the European Communities Sixth Framework Programme (EURATOM).

[1] T. H. Stix, *Waves in Plasmas* (Springer-Verlag, New York, 1992).
[2] I. Bernstein, Phys. Rev. **109**, 10 (1958).
[3] J. Preinhaelter and V. Kopecký, J. Plasma Phys. **10**, 1 (1973).
[4] E. Mjølhus, J. Plasma Phys. **31**, 7 (1984).
[5] H. P. Laqua *et al.*, Phys. Rev. Lett. **78**, 3467 (1997).
[6] V. Shevchenko *et al.*, in *Radio Frequency Power in Plasmas*, edited by C. Forest, AIP Conf. Proc. No. 694 (AIP, New York, 2003), p. 359.
[7] G. Taylor *et al.*, Phys. Plasmas **12**, 052511 (2005).
[8] P. K. Chattopadhyay *et al.*, Phys. Plasmas **9**, 752 (2002).
[9] V. Shevchenko, Y. Baranov, M. O'Brien, and A. Saveliev, Phys. Rev. Lett. **89**, 265005 (2002).
[10] S. Shiraiwa *et al.*, Phys. Rev. Lett. **96**, 185003 (2006).
[11] F. Wagner *et al.*, Phys. Rev. Lett. **49**, 1408 (1982).
[12] F. Volpe, Ph.D. thesis, Ernst-Moritz-Arndt-Universität Greifswald, Germany [IPP Report No. 13/1, 2003].
[13] F. Volpe and H. P. Laqua, Rev. Sci. Instrum. **74**, 1409 (2003).
[14] A. Manini *et al.*, Plasma Phys. Controlled Fusion **44**, 139 (2002).